

**TECHNOLOGY INTEGRATION BOX BEAM FAILURE STUDY:  
STATUS REPORT**

M. J. Shuart, D. R. Ambur, D. D. Davis, Jr.,  
R. C. Davis, G. L. Farley, C. G. Lotts, and J. T. Wang

56-39

51346

P-13

**Introduction**

Composite structures have the potential to be cost-effective, structurally efficient primary aircraft structures. The Advanced Composites Technology (ACT) Program has the goal to develop the technology to exploit this potential for heavily loaded aircraft structures. As part of the ACT Program, Lockheed Aeronautical Systems Company completed the design and fabrication of the Technology Integration Box Beam (TIBB, ref. 1). The TIBB is an advanced composite prototype structure for the center wing section of the Lockheed C-130 aircraft. Lockheed tested the TIBB for downbending, upbending, torsion, and combined upbending and torsion load conditions to verify the design (ref. 2). The TIBB failed at 83 percent of design ultimate load for the combined upbending and torsion load condition.

The objective of this paper is to describe current results from an on-going study of the mechanisms that led to the failure of the TIBB. Experimental and analytical results are presented. Experimental results include load, strain, and deflection data for the TIBB. An analytical investigation was conducted to compliment the experimental investigation and to gain additional insight into the TIBB structural response. Analytical results include strain and deflection results from a global analysis of the TIBB. A local analysis of the failure region is being completed. These analytical results are validated through comparisons with the experimental results from the TIBB tests. The experimental and analytical results from the TIBB tests are used to determine a sequence of events that may have resulted in failure of the TIBB. A potential cause of failure is high stresses in a stiffener runout region. Typical analytical results are presented for a stiffener runout specimen that is being defined to simulate the TIBB failure mechanisms. The results of this study are anticipated to provide better understanding of potential failure mechanisms in composite aircraft structures, to lead to future design improvements, and to identify needed analytical tools for design and analysis.

**PRECEDING PAGE BLANK NOT FILMED**

## Applied Loads and Reactions for Failure Load Case

The TIBB loading conditions were thoroughly examined as a precursor to understanding the TIBB response and failure mechanism. The TIBB was loaded at both ends of the beam and was supported by mainframes in the middle of the beam as illustrated at the top of figure 1. Loads were applied to the TIBB using hydraulic actuators located at four corners of the TIBB. Applied loads measured during the test are shown on the left side of the figure. The applied loads for the forward right and left actuators were equal, and the applied loads for the aft right and left actuators were equal. The applied loads for the forward actuators were 230 percent greater than the applied loads for the aft actuators to simulate a combined upbending and torsion wing-loading condition. This loading condition will be referred to herein as the failure load case. Loads were applied to the TIBB incrementally during the test, and selected strain and displacement results were evaluated at each load level. The "stair-step" trend for the applied load data is a result of the applied loading procedure.

Results for the reaction forces in the TIBB mainframe supports are shown on the right side of figure 1. Each reaction force was calculated using results from strain gages located on the corresponding mainframe support. Results for the reaction forces are shown on the figure as percentages of the total load. The percentage of the total load for each reaction force varied significantly for total loads below 50 kips. The variations are due to settling of the test fixture and TIBB during loading. At failure (i.e., 301 kips total applied load) the forward right and left reaction loads were approximately 50 and 20 percent, respectively, of the total load, and the aft right and left reaction loads were approximately 20 and 5 percent, respectively, of the total load. The calculated reaction forces were expected to have a load distribution similar to that for the applied loads. The results for the calculated reaction forces may be affected by the boundary conditions at the supports, deformation of the test fixture, and/or rigid body motions of the TIBB.

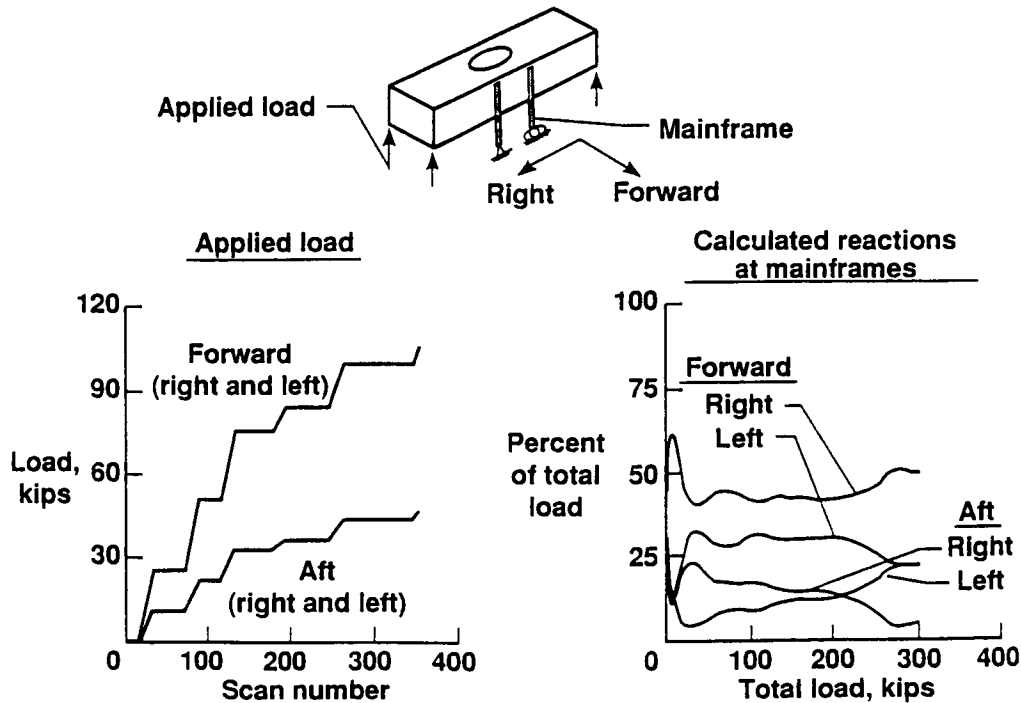


Figure 1

## Typical Strains in the Upper Cover

Measured axial strains for the failure load case from the upper cover of the TIBB are shown in figure 2. Strain gage locations are identified by the letters A through F and are indicated by a parallelogram on the schematic at the top of the figure and by the sketch of stiffener cross sections at the lower right of the figure. The approximate location of the TIBB failure across the upper cover is also indicated on the schematic. The strain gages at location C are in the vicinity of a hat stiffener, and the strain gages at location D are in the vicinity of a blade stiffener. The subscripts i and e for the letters C and D designate strain gage locations on the interior and exterior surfaces, respectively, of the TIBB.

Axial (spanwise) strain results are plotted on the figure as a function of the total applied load. The strains at locations A, B, E, and F are consistent with the expected deformation of the TIBB for this load case. The largest axial compressive strain is approximately -0.0045 in./in. and occurs at location E. The differences between the interior surface strains and the exterior surface strains at locations C and D indicate stiffener bending. Severe bending in the hat stiffener at failure is caused by local bending moments near the termination of the hat stiffener.

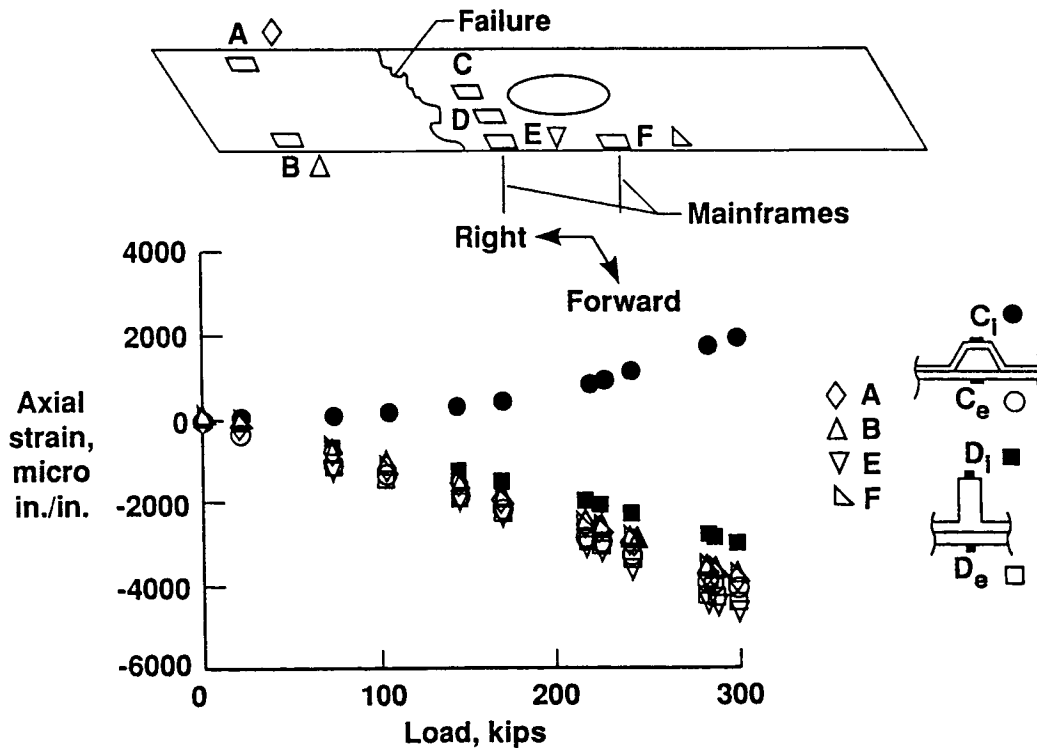


Figure 2

### Typical Strains in the Forward Spar

Measured axial strains for the failure load case from the forward spar of the TIBB are shown in figure 3. Strain gage locations are identified by the letters A through F and are indicated by a rectangle on the schematic at the top of the figure. The schematic also includes the approximate location of the TIBB failure across the forward spar. Strain results are plotted using the symbol identified for each letter in the legend on the right side of the figure. The open symbols correspond to results for gages located near the upper cover of the TIBB, and the filled symbols correspond to results for the gage located near the lower cover. Strain results for locations A and B indicate upbending of the spar which is consistent with this load case. The maximum compressive strain at location A is approximately -0.0046 in./in. The maximum measured compressive strain for the forward spar is at location C and is approximately -0.006 in./in. This maximum compressive strain is too low to cause failure of this undamaged structure. Furthermore, the TIBB failure propagates through a region of the spar where the compressive strains are even lower. These experimental results and similar results for the aft spar indicate that the TIBB failure may have initiated in the upper cover.

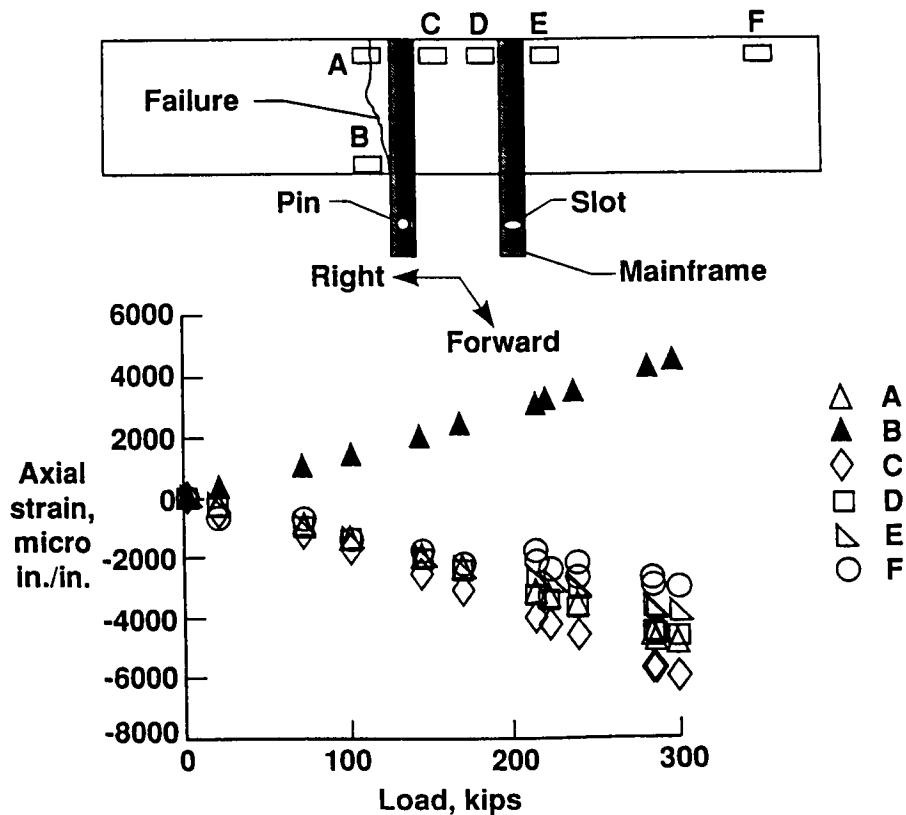


Figure 3

## **Analytical Approach**

An analytical investigation of the TIBB is being conducted to complement the experimental investigation and to gain additional insight into the TIBB structural response. The analytical approach used in this study is summarized in figure 4. Analyses are being conducted using the MSC/NASTRAN (ref. 3) and the Computational Mechanics Testbed (COMET, refs. 4, 5) finite element computer codes. Global analyses for the entire TIBB are being performed using MSC/NASTRAN. The results from the global analyses are being verified using the available experimental results. Displacement results from the verified global analyses will be used as input to a local analysis of the upper cover failure region. The local analysis is being performed using COMET. The local analysis will be used to obtain detailed deformation and strain distributions. The local analysis results will be verified using available experimental results.

A potential test specimen for this TIBB study will also be analyzed. This specimen is referred to herein as the stiffener runout specimen and will be described subsequently in this paper. Analyses for the stiffener runout specimen will be conducted to determine the specimen's response to compression loading for comparison to the TIBB's response to the failure load case. Specimen geometry and loading conditions for the stiffener runout specimen will be evaluated analytically to determine the response that best approximates the TIBB's response at failure. The deformation and strain distributions for the stiffener runout specimen will be predicted prior to testing.

- **Use the Computational Mechanics Testbed (COMET) and MSC/NASTRAN**
- **Conduct global analysis of TIBB; verify global analysis with experimental results**
- **Use displacement results from verified global analysis as input boundary conditions for local analysis of upper cover**
- **Conduct local analysis of failure region to determine deformations, strains; verify local analysis with experimental results**
- **Analyze stiffener runout specimen**
  - **simulation of TIBB failure mode**
  - **specimen geometry, test conditions**
  - **predict deformations, strains**

Figure 4

## Axial Surface Strain for Failure Load Case from Modified Global Analysis

Axial surface strain distributions obtained from a modified MSC/NASTRAN global model of the TIBB are shown in figure 5 for the failure load case. The model used for the present analysis was based on a model developed by Lockheed for the TIBB and has been modified to include stiffener runouts and flanges of hat stiffeners. The present global finite element model is more detailed than the original Lockheed model. The present model contains 3,885 quadrilateral, triangular, and bar elements and has 16,578 degrees of freedom.

The global analyses were used to calculate strains in regions near the observed failure. The exterior surface strain distribution is shown on the TIBB global model near the top of the figure. These results do not indicate any unusually high exterior surface strains. A portion of the interior surface strain distribution is shown in the lower half of the figure. The interior surface strain distribution is presented for the upper cover region near the observed failure. These results show strains for the skin of the upper cover that are greater than  $-0.01$  in./in. in the region of the hat stiffener termination. The high skin strains are caused by an eccentric load path that induces local bending. The observed TIBB failure extends through the region of the hat stiffener termination.

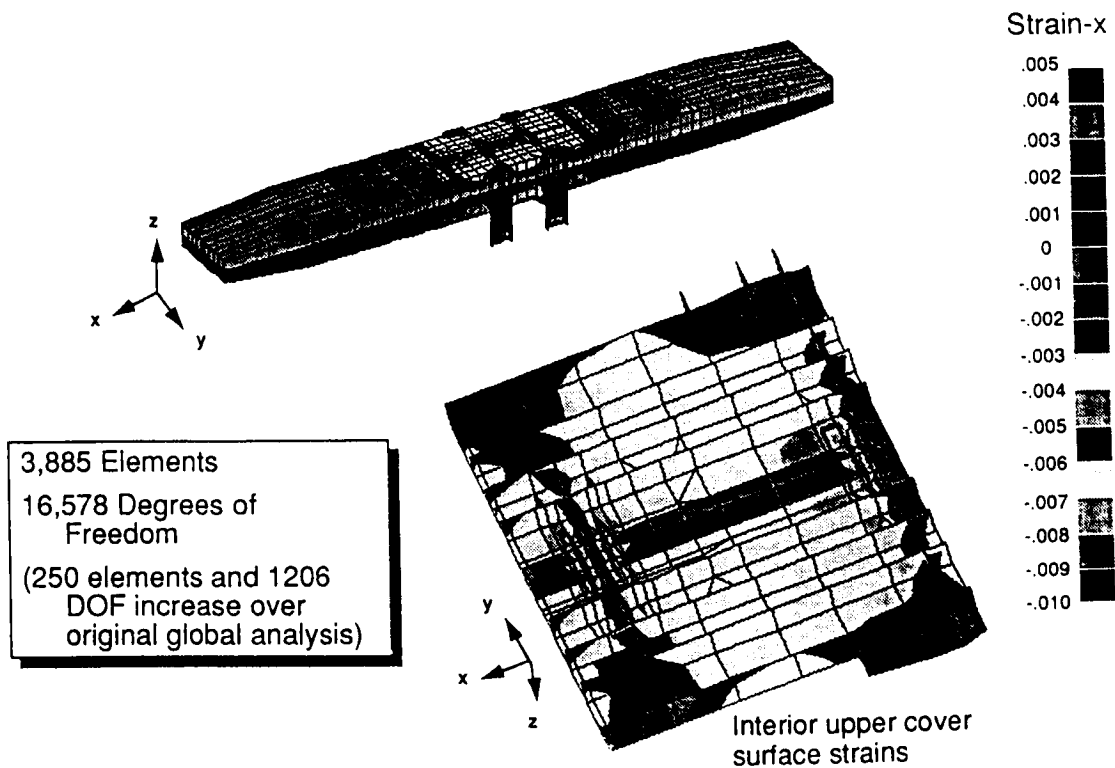


Figure 5

## Vertical Spar Deflections for Failure Load Case

The vertical deflections for the forward and aft spars predicted by the global analysis are compared with experimental results in figure 6. Measured deflections for the left and right ends of the TIBB ( $\eta = \pm 206.6$  in., respectively) and for the mainframes were used as boundary conditions for the global analyses. The composite test section of the TIBB is located between wing stations  $\eta = \pm 75$  in. Correlation between the measured and predicted deflections is excellent.

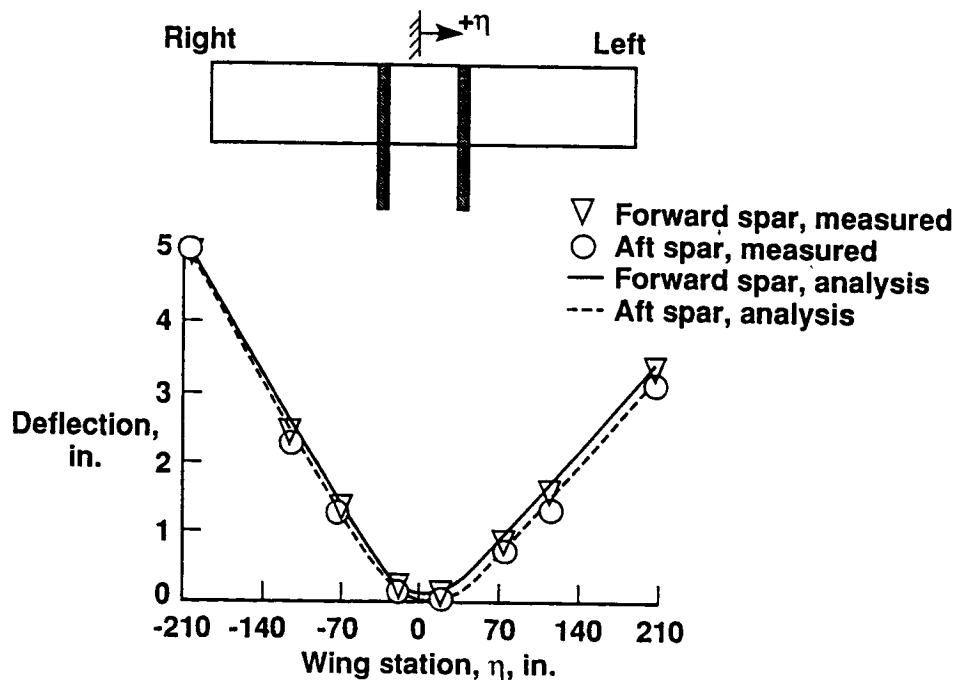


Figure 6

## Upper Cover Axial Strains at Failure

A comparison of upper cover strains at failure of the TIBB is presented in figure 7. Measured strains are compared to predicted strains from the global analysis, and all strains are given in units of micro-in./in. The experimental and predicted strains are shown in the figure at the approximate strain gage location on a schematic of the upper cover. The results on the figure indicate good agreement between test and analysis strains for gages located near the center of the upper cover. The results indicate poor agreement between test and analysis strains for gages located near the ends of the upper cover. These differences between experimental and predicted results may be due to modeling approximations for the TIBB load introduction structure. The results on the figure also indicate poor agreement between test and analysis strains for gages located near the mainframe supports that may be due to modeling approximations for the mainframe, spar, and upper cover connections. Despite the modeling approximations, the experimental and analytical results for the global model agree reasonably well in the center of the upper cover.

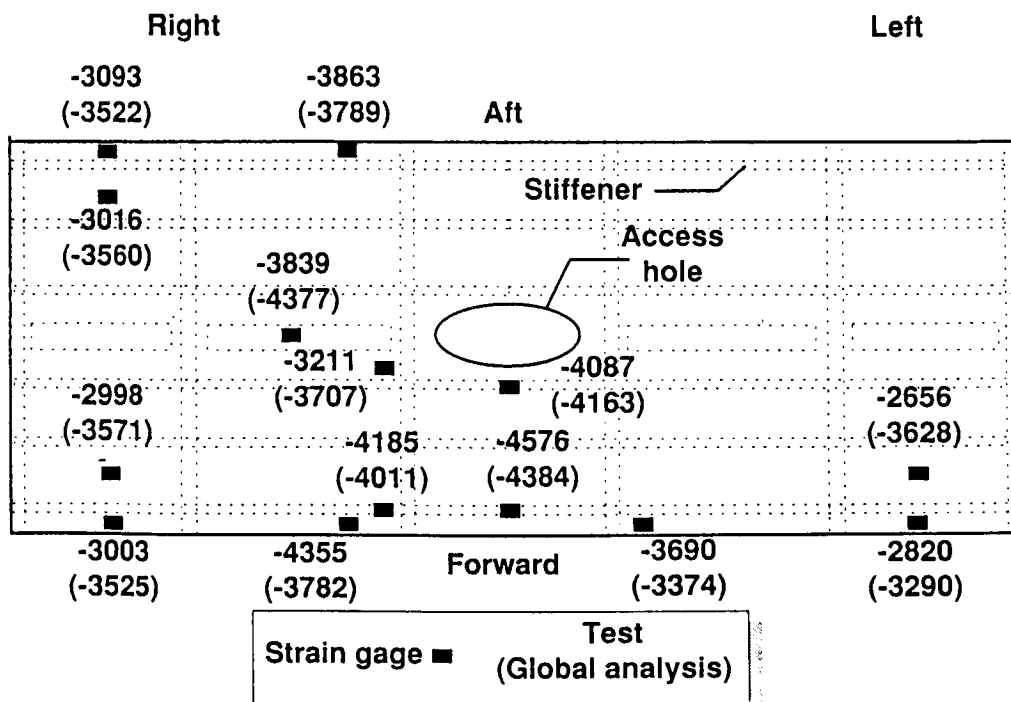


Figure 7

## Finite Element Model for Local Analysis

A detailed local finite element model of half of the upper cover was developed to determine the deformations and strains near the TIBB failure. The local model shown in figure 8 consists of 4,338 9-noded assumed natural-coordinate strain elements (ref. 6) resulting in approximately 88,000 degrees of freedom. Several loading conditions will be used to investigate the behavior of the upper cover. Displacements and rotations from the global analysis will be applied along all four edges of the local model and at the locations where the transverse ribs attach to the cover skin.

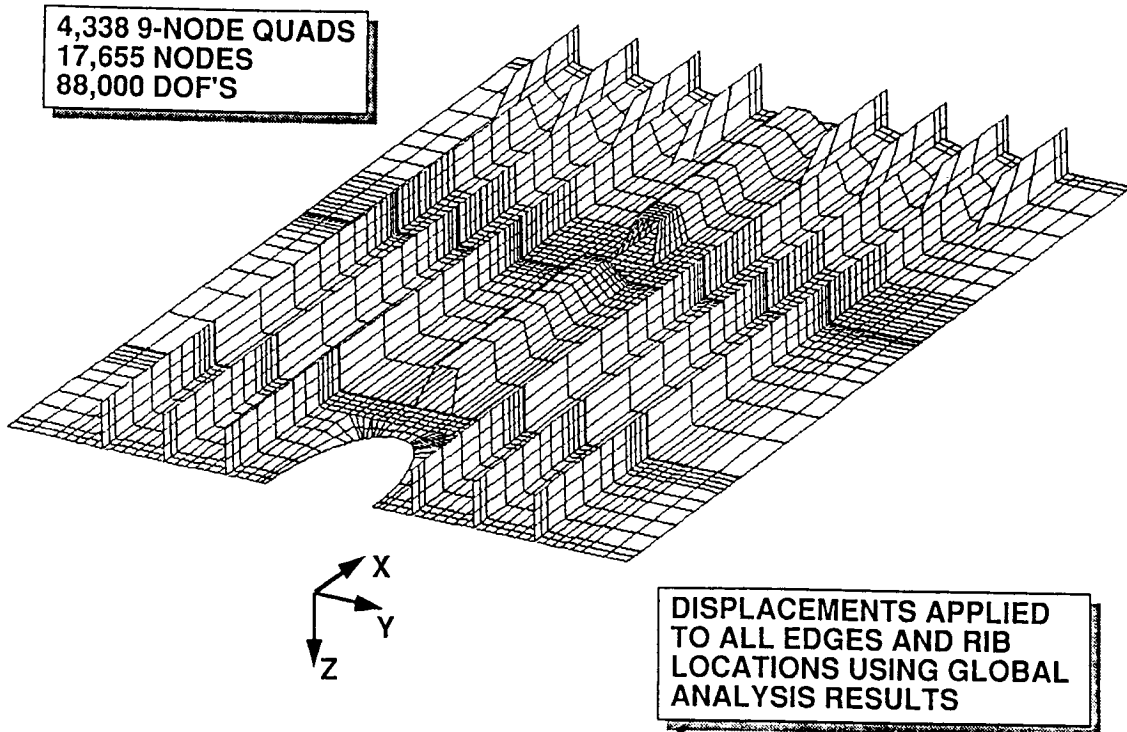


Figure 8

## **Preliminary Failure Scenario**

Experimental and analytical results from this study have been combined to determine a preliminary failure scenario that is summarized in figure 9. When the TIBB was subjected to the failure load case, the eccentric load path at the hat stiffener termination resulted in local bending moments. These bending moments produced severe bending deformations in the hat stiffener and in the unsupported skin near the hat stiffener termination. The unsupported skin also experienced large axial strains due to the thickness discontinuity caused by termination of the stiffener flanges. A combination of large axial and bending strains in the unsupported skin at the hat stiffener termination initiated the failure of the skin of the TIBB upper cover. This failure propagated in the chordwise direction across the TIBB upper cover and caused the forward and aft spars to fail.

- **Combined bending/torsion loading applied to TIBB**
- **Hat stiffeners subjected to severe bending**
- **Unsupported skin at hat stiffener runout subjected to severe bending**
- **Strains in skin at stiffener runout initiated TIBB failure**
- **Upper cover failure led to forward and aft spar failures**

Figure 9

## Stiffener Runout Test Specimen

A stiffener runout test specimen (SRTS) was cut from the undamaged portion of the TIBB upper cover as illustrated by the schematic in the upper left of figure 10. The SRTS is approximately 60 in. long and 33 in. wide and will be tested in uniaxial compression to verify the preliminary failure scenario. The unloaded edges of the SRTS will be constrained with knife edges to simulate a simple support boundary condition. The out-of-plane deflection  $w$  will be constrained to be zero along the transverse rib connection located near the center of the specimen. Approximately 150 strain gages and 10 direct current differential transformers (DCDT's) will be used to measure the SRTS response to the applied load. Strains in the critical region of the unsupported skin between the hat stiffener termination and the transverse rib flange will be measured using strain gages and full-field laser interferometry techniques.

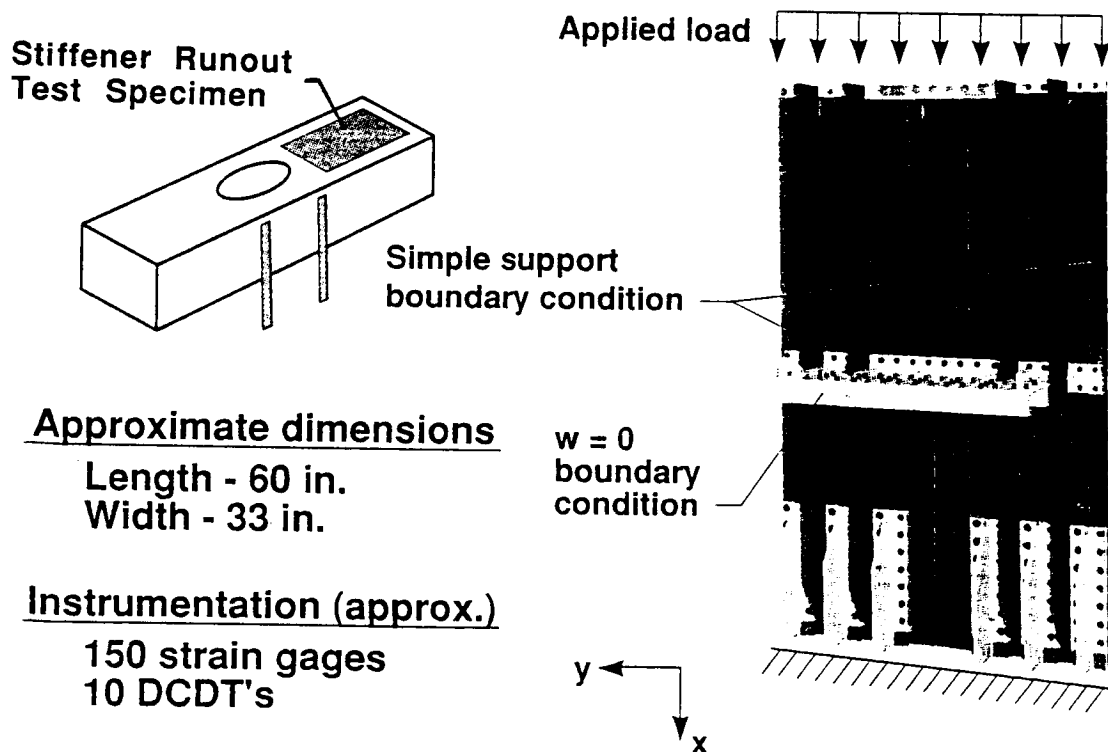


Figure 10

## Typical Response of Stiffener Runout Test Specimen

The stiffener runout test specimen (SRTS) will be tested to simulate the TIBB response and failure mechanisms and thereby verify the TIBB failure scenario. A finite element analysis of the SRTS is being conducted to study the effects of specimen geometry, intermediate supports, end fixity, and depth of end potting on the specimen behavior. A half-model of the SRTS is being developed. Preliminary results from these analyses indicate that regardless of end fixity or depth of end potting, very high strains exist in the unsupported skin near the hat stiffener termination. A typical response for the SRTS is shown in figure 11. Deformed geometry and load-shortening response are shown on the figure. Significant bending deformation of the hat stiffener and the upper cover skin are illustrated.

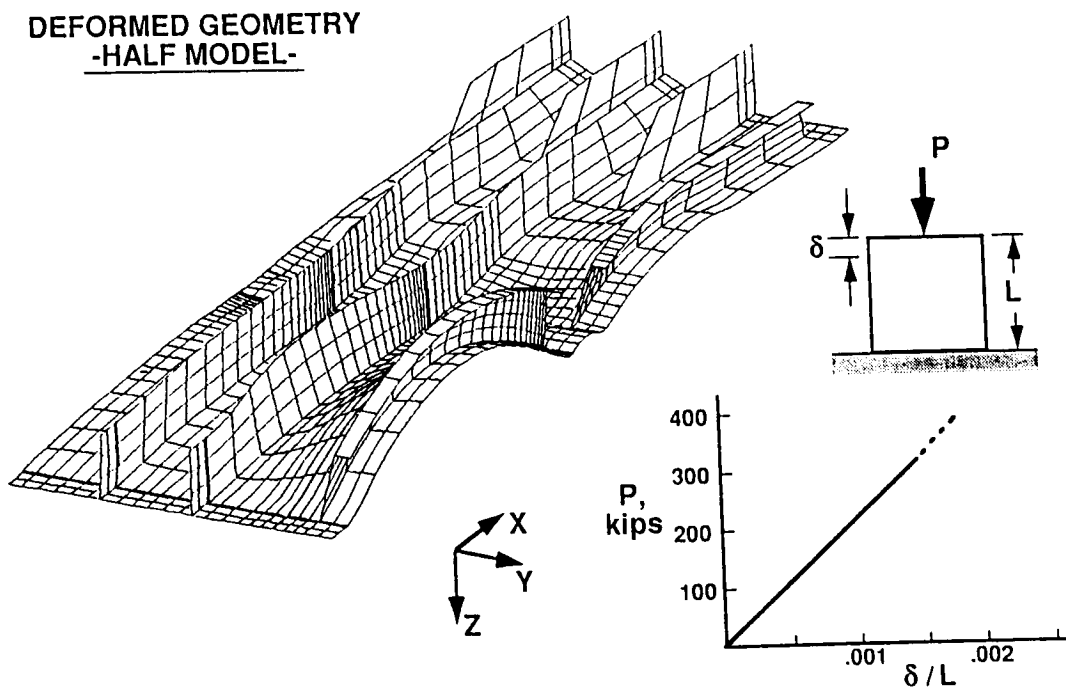


Figure 11

## Concluding Remarks

A comprehensive experimental and analytical study is underway to quantify the mechanisms that led to the failure of the Technology Integration Box Beam (TIBB). The experimental results indicate significant bending deformation of the hat stiffener and upper cover skin. Analytical results from a modified global model of the TIBB agree reasonably well with experimental results. Additional analysis is being conducted using a local model of the TIBB upper cover which includes the failure region. Preliminary results from this study suggest that failure of the TIBB initiated in the upper cover skin due to severe bending of the upper cover skin in the region of the hat stiffener termination. A stiffener runout specimen is being defined to simulate the TIBB response and failure mechanisms.

## References

1. Griffin, C.; and Meade, L.: Design, Analysis and Fabrication of the Technology Integration Box Beam. Proceedings of the First NASA Advanced Composites Technology Conference, Seattle, WA, October 29-November 1, 1990, NASA CP-3104, Part 1, 1991, pp. 157-178.
2. Griffin, C. F.: Structural Testing of the Technology Integration Box Beam. Presented at the 9th DoD/NASA/FAA Conference on Fibrous Composites in Structural Design, Lake Tahoe, NV, November 4-7, 1991.
3. MSC/NASTRAN User's Manual, Version 65, Vols. 1 and 2. The MacNeal-Schwendler Corporation.
4. Knight, N. F., Jr.; and Stroud, W. J.: Computational Structural Mechanics: A New Activity at the NASA Langley Research Center. NASA TM 87612, 1985.
5. Lotts, C. G.; Greene, W. H.; McCleary, S. L.; Knight, N. F.; Paulson, S. S.; and Gillian, R. E.: Introduction to the Computational Structural Mechanics Testbed. NASA TM 89096, 1987.
6. Park, K. C.; and Stanley, G. M.: A Curved  $C^\circ$  Shell Element Based on Assumed Natural-Coordinate Strains. Journal of Applied Mechanics, vol. 53, 1986, pp. 278-290.